Controllable polarization insensitive and large-angle beam switching with phase-change metasurfaces

Arash Nemati [1#], Guanghui Yuan [2#], Jie Deng [1], Aihong Huang [1], Weide Wang [1], Toh Yeow Teck [1], Jinghua Teng [1*] and Qian Wang [1*]

[1] *Institute of Materials Research and Engineering, Agency for Science, Technology and Research (A*STAR), 2 Fusionopolis Way, Innovis 08-03, 138634, Singapore*

[2] *Department of Optics and Optical Engineering, University of Science and Technology of China, Hefei, Anhui 230026, China*

Abstract

The development of high-efficiency compact non-mechanical beam tuning devices has attracted a lot of attention for LiDAR, AR display, and chip-to-chip communication. Owning to the fast wavefront manipulation in an ultra-thin dimension, metasurfaces have been regarded as potential substitutes for traditional tunable optical components towards further miniaturization and low power consumption. However, most beam tuning metasurfaces currently are polarization-sensitive and designed to work in reflection mode, which limits their applications in integrated optical systems for full-range steering. In this paper, a transmission mode polarization insensitive beam switching metasurface based on nonvolatile phase-change material $Ge_2Sb_2Te_5$ was proposed and experimentally demonstrated at the telecommunication wavelength. The high transmission efficiency with a large switching angle of up to 75° is achievable for potentially full-range beam steering applications. As a proof of concept, the transmitted beam with a switching angle of 15° and directivity of 82.4% was demonstrated. In addition, by controlling the phase transition in the intermediate states, the metasurface can be used as a tunable beam splitter to control the ratio of the beam power between two predesigned transmission angles. The demonstrated phase-change metasurfaces pave the way for achieving high-efficiency dynamic beam steering for various important applications.

1. Introduction

Beam switching and steering is one of the core functions in optical devices and systems. The new applications that have emerged recently, such as light detection and ranging (LiDAR) sensors, wearable augmented reality displays, or chip-to-chip communications, demand new beam control devices with improved speed, low energy consumption, and high integration capabilities [1-5]. Unlike conventional devices that rely on bulky optomechanical components for control of light refraction, reflection, and transmission, metasurfaces offer flexibility to control the beam wavefront using subwavelength nanostructure which can support strong dielectric or plasmonic electromagnetic resonance [6-11]. Recently, metasurfaces have been designed to exhibit superior advantages to realize ultra-thin beam tuning functions for various applications [12-18]. Metasurface has presented a versatile solution for multi-functional active beam control through various external stimuli, such as mechanical force [19-21], thermal-optic [22-24], free carrier [13, 25-28], electro-optic [29-32], and all-optical approaches [33-35], where active materials with attractive thermal, optical, or electric properties play a crucial role.

$Ge_2Sb_2Te_5$ (GST), a phase change material based on chalcogenide alloys, is traditionally used in rewritable optical disks and phase change memory applications [24]. Recently, it has attracted a lot of attention as an optical material with unusual characteristics, in particular, significantly large and reversible refractive index change between the amorphous and the crystalline states [36-41]. The non-volatile phase transition of GST makes it interesting in tunable nanophotonic devices. In the past several years, various non-volatile reconfigurable phase change metadevices using GST exhibited controllable reflective beam switching and steering in the near IR region [42-46]. However, these approaches are either polarization-sensitive, coming with the price of increased complexity in system integration, or only work in the reflection mode which dramatically limits their practical usages. Therefore, a high-efficiency tunable optical metasurface switch capable of controlling the phase of beam wavefront for various incident polarization states, particularly in the transmission mode, is desired for active photonics applications.

In this work, we propose a controllable beam switching device based on all-dielectric phase change material metasurface operated in the transmission mode. At the telecommunication wavelength ($\lambda \sim 1550\ nm$), amorphous GST (a-GST) has a very low optical loss ($n_a = 3.88 + 0.016i$) while crystalline GST (c-GST) is lossy ($n_c = 6.09 + 0.83i$). Theoretically, a-Si nanorod

meta-gratings have been demonstrated for continuous beam steering through coherent illumination with two counter-propagating beams [47]. In this work, the subwavelength GST nanorods in the amorphous state guide the light beam for the desired switching angle θ (for example $\theta = 15°$) using the waveguide mode, where the phase shift depends on the effective index of the unit cell. As the phase of GST nanorods changes to crystalline under external excitation, they become lossy, and the incident beam is partially absorbed in the nanorods and the waveguide mode disappears. Therefore, the remaining incident laser beam would pass through the metasurface without any deflection ($\theta = 0°$). Since the diameter of nanorods in the supercell is relatively small and the thickness is relatively thin, the transmission efficiency of the all-dielectric tunable metasurface is high. Unlike the conventional metasurface grating, the nanorod design we proposed and demonstrated in this work is polarization insensitive. In addition, the ratio of laser intensity between $\theta = 15°$ and $\theta = 0°$ could be controlled by accurately changing the phase of the GST nanorods. Our simulation and experimental results show control over the intensity of the transmitted beam at both angles.

2. Result and Discussion

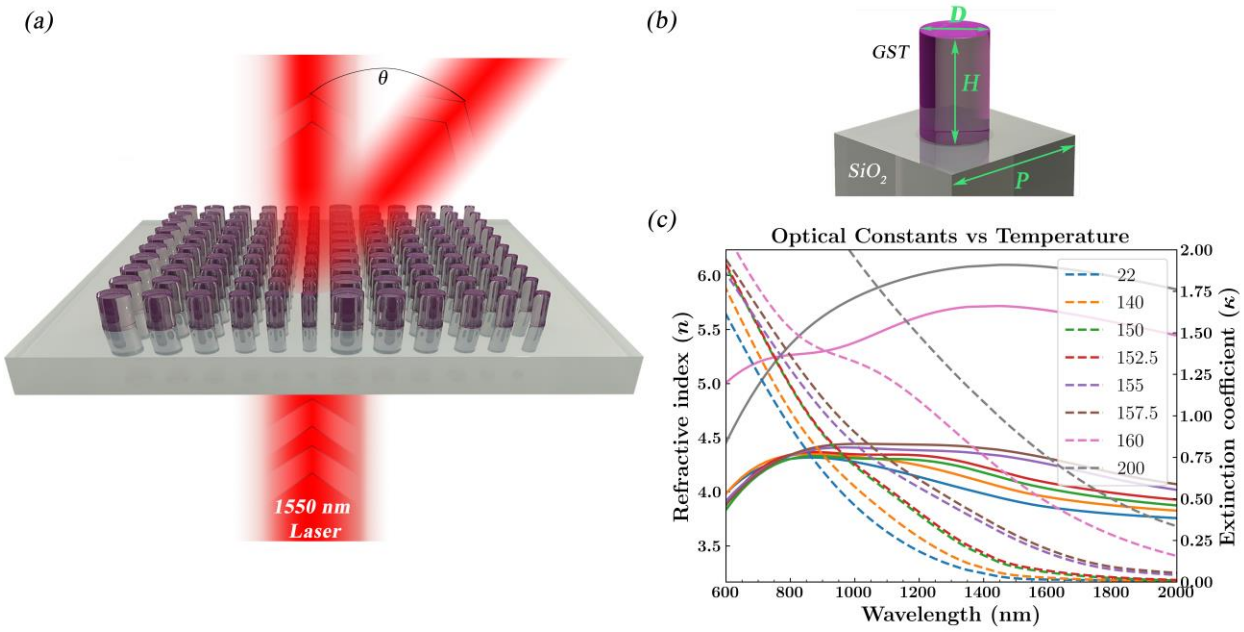

Figure 1. (a) Schematic of the polarization-insensitive beam switching phase-change metasurface. The designed metasurface switches the laser beam at the wavelength of 1550 nm between 0 and $\theta°$ with phase transition of GST from amorphous to crystalline. (b) Square unit-cell of the metasurface comprising quartz (SiO_2) substrate and a circular GST nanorod. The dimensions of the unit cell are *P*, *H*, and *D* for the

unit cell's period, nanorod's height, and diameter, respectively. (c) Experimental characterization of refractive index (*n, solid line*) and extinction coefficient (*k, dashed line*) of the GST films using a variable angle spectroscopic ellipsometer. The GST thin film of 650 nm thickness is placed on a hotplate at a different temperature from 140 °C to 200 °C for two minutes to achieve the gradual phase transition from amorphous to crystalline.

Figure 1 (a) shows the schematic of the proposed tunable polarization insensitive beam switching metasurface based on the GST phase change material. The circular GST nanorods array is patterned on a quartz substrate. The amplitude and phase of the transmitted beam of each nanorod could be controlled by changing the height (H) and diameter (D) of GST nanorods, as shown in Figure 1(b). As mentioned in the previous section, the GST in the amorphous phase has a slight loss at $\lambda = 1550$ nm. Hence, a tunable metasurface to deflect the transmitted laser to the desired angle ($\theta°$) could be designed by creating a progressing phase shift by changing the diameter of GST nanorods. If the phase of the GST film changes from amorphous to crystalline, the optical constants of the GST nanorods would change and the designed progressive phase shift would be disturbed. Moreover, due to the loss of crystalline GST, the laser beam entering the GST nanorods would not guide through it in a waveguide mode. The phase shift of the transmitted beam for the different diameters of c-GST nanorods is much smaller than that of a-GST nanorods. Hence, the metasurface would transmit the beam without any deflection.

Figure 1(c) shows the refractive index (n) and extinction coefficient (k) of 650 nm thickness GST film measured by a variable angle spectroscopic ellipsometer. As the temperature rises, the GST phase changes from an as-deposited amorphous state to a crystalline state [48, 49]. A precision temperature-controlled hotplate is used for gradual phase transition. Above 160 °C, the optical properties of GST do not change much due to complete crystallization. In the simulations, we consider GST heated to 200 °C as a fully crystalline state.

Ideally, the metasurface design requires a continuous phase distribution of 2π with a uniform high transmission amplitude for perfect control [50]. For a desired one-dimensional deflection angle of $\theta°$, the linear progressive phase profile of the unit cells in the metasurface should be $\psi(x) = (2\pi/\lambda)p \sin\theta$, where λ is the operational wavelength, p is the period of grating on the metasurface [51]. We design the metasurface with a deflection angle of 15°. There are 11 unit cells in each super-cell period to cover the 2π phase distribution in a $2\pi/11$ discrete phase step. The calculated grating period is 5995 nm and the unit cell period is 545 nm. The feature size of each

unit cell is optimized to obtain the desired phase shift for patterning the metasurface. The simulations are done by sweeping the diameter of the GST nanorod while other parameters such as nanorod's height and unit cell's period are kept constant. Moreover, since circular nanorods are used the metasurface is insensitive to the polarization of the incident beam.

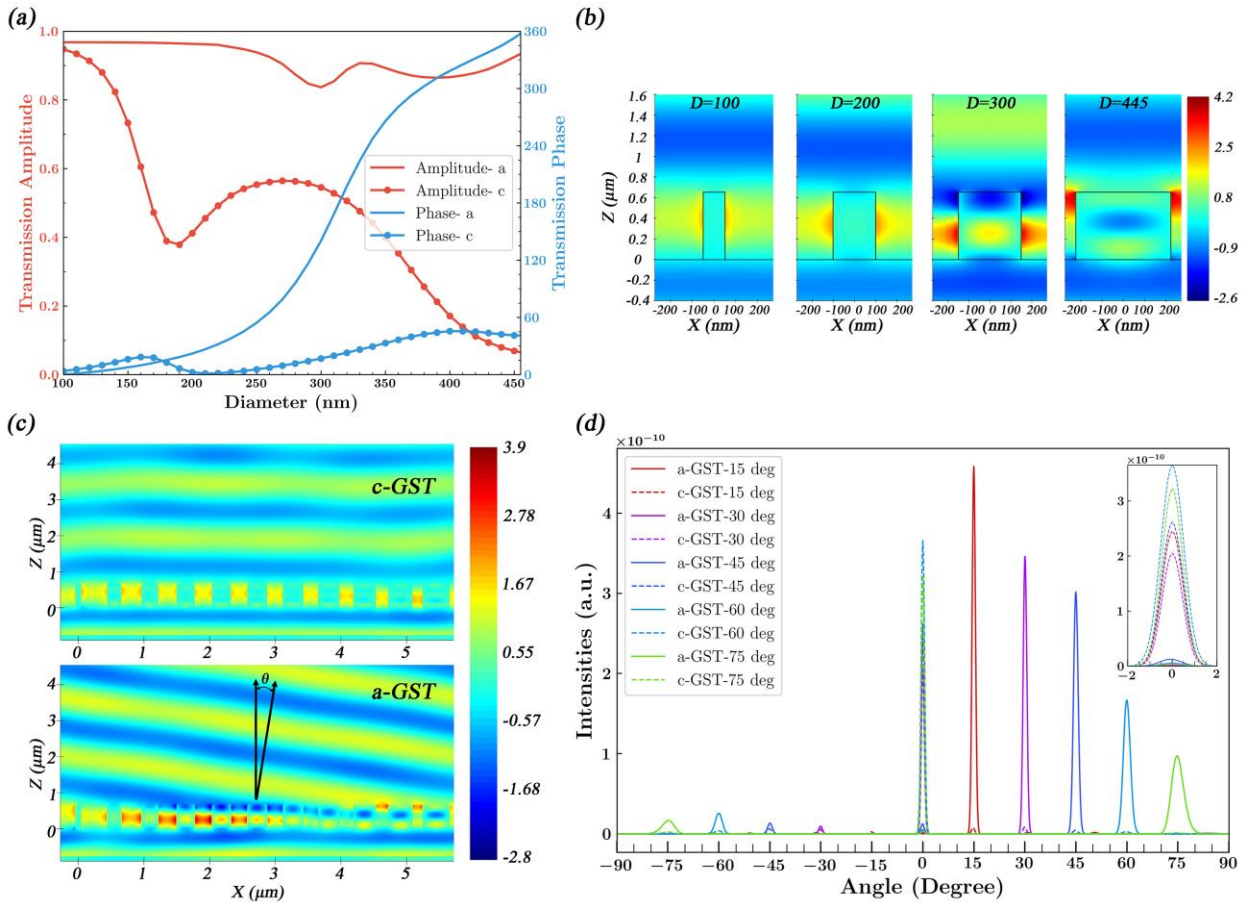

Figure 2(a) Lumerical FDTD simulation results of amplitude (red line) and phase (blue line) of the transmitted beam of GST unit cell (amorphous and crystalline) as the diameter is swept from $D = 100$ nm to $D = 445$ nm, and the height is 650 nm. (b) The electric field (Ex) distribution of amorphous GST nanorods with diameters of 100 nm, 200 nm, 300 nm, and 445 nm, respectively. (c) The simulated wavefront of the transmitted beam (Ex) of the metasurface super-cell with horizontal-polarized incident light. Diameters of nanorods in the supercell are 150 nm, 236 nm, 268 nm, 288 nm, 302 nm, 314 nm, 326 nm, 338 nm, 356 nm, 386 nm, 434 nm and the period of 11 square unit cells is 545 nm. (d) The simulated far-field intensity ($|E|^2$) of the phase-change metasurfaces in the amorphous and crystalline states for deflection angles of 15°, 30°, 45°, 60°, and 75°, respectively. The period and height of each design are constant and the diameter of GST nanorods are chosen to satisfy the phase and amplitude requirements of beam switching and tuning. The details of designs are: 15° [P=545nm, H=650 nm], 30° [P=516 nm, H=700 nm]; 45° [P=548 nm, H=700 nm]; 60° [P=596 nm, H=700 nm]; 75° [P=535, H=700 nm] Inset is the enlarged figure of beam intensity of normally transmitted beam at 0°.

Figure 2(a) shows the results of Lumerical FDTD simulations of transmission amplitude and

phase of each unit cell as the diameter of GST nanorod (amorphous and crystalline) is increased from 100 nm to 445 nm (5 nm step sizes). The height of 650 nm nanorod is used after optimization to meet the phase distribution requirement of the metasurface. A maximum phase shift of 360º is achieved with a diameter of 455 nm, which is sufficient to design a progressive phase distribution for high-efficiency metasurface. Hence, to pattern the metasurface, the diameter of nanorod in each unit cell along the X-axis is chosen from Figure 2(a) to satisfy the required phase shift, while the unit cell along the Y-axis is repeated with the same size.

To investigate the phase shift in the unit cell with GST nanorods with $H = 650$ nm in more detail, the electric field profiles (*Ex*) in the X-Z plane for different diameters of GST nanorods are shown in 2(b). As the diameter of the nanorod is increased from 100 nm to 445 nm, the electric field profiles show shorter periods which implies higher effective indices. In other words, the effective refractive index along the propagation direction (Z-axis) increases, resulting in greater phase retardation, as shown in Figure. Moreover, the slight resonance inside the GST nanorod at D =300 nm is observed due to the slightly confined magnetic dipole mode existing in the GST nanorod. This resonance corresponds to the decrease in the transmission amplitude in Figure 1(a). It may affect the efficiency of the metasurface designed for large deflection angle, which can be compensated using optimization algorithms such as particle swarm optimization algorithm [52].

Figure 2(c) shows the simulated wavefront of the transmitted beam after the supercell of metasurface in amorphous and crystalline states which is designed to deflect the beam toward 15º. The in-plane illumination light source is normal to the metasurface. The transmitted beam is deflected 15° in the amorphous state of the GST metasurface. After the complete phase transition to the crystalline state, the metasurface guides the incident beam without any deflection.

Figure 2 (d) shows the Lumerical FDTD simulation results for the far-field intensity of the metasurfaces with the different designs for beam tuning angles of 15°, 30°, 45°, 60°, and 75°, respectively. For each metasurface design, we use a similar strategy to optimize the period, height, and diameter of each unit cells. The far-field projection function in FDTD is used to simulate the far-field distribution of meta-grating illuminated by the Gaussian beam. In Figure 2(d) the far-field intensity in amorphous and crystalline phases of the metasurface is shown in solid line and dash line, respectively. The metasurface deflects the transmitted beam almost completely to the desired angle, such as 15º, in the amorphous phase. By changing the phase of GST film to crystalline phase,

the progressive phase change is distorted and the transmitted beam has nearly no deflection. This is achieved by changing the complex refractive index of all GST nanorods from amorphous to crystalline in the simulations. The figure-of-merit (FOM) for a beamsteering metasurface is defined as [52]:

$$FOM = \frac{\int_{\theta_1}^{\theta_2} |E(\theta)|^2 d\theta}{\int_{-\pi/2}^{\pi/2} |E(\theta)|^2 d\theta} \times T \times 100 \qquad 1$$

Where $E(\theta)$ is the far-field angular electric field distribution on the hemisphere, θ_1 and θ_2 are chosen to be at the midpoints to the adjacent grating orders, and T is the transmission efficiency of the metasurface. The FOM which ranges from 0% to 100%, shows what percentage of the forward transmitted beam is directed toward the desired deflection angle (here main lobe θ°). The calculated FOMs of phase-change metasurface are 88.2% at 15° beam deflection (amorphous state) and 45.5% at 0° (crystalline state). The modulation depth of 0.98 is achieved for 15º beam switching.

θ°	a-GST			c-GST		
	Transmission (%)	FOM (θ °)	FOM (0 °)	Transmission (%)	FOM (θ °)	FOM (0 °)
15	89.2	88.16	0.08	48.46	1.41	45.52
30	81.19	77.72	0.42	43.7	1.85	40.27
45	86.78	80.88	2.35	52.31	1.18	49.46
60	71.07	60.76	0.97	68.74	0.95	66.38
75	82.33	68.97	0.71	62.83	0.91	60.3

Table 1: The calculated transmission efficiency and FOM of phase-change metasurface for beam switching with deflection angles of 15°, 30°, 45°, 60°, and 75° respectively.

Table 1 shows the calculated transmission efficiency *T*, and FOM of phase-change metasurface designed for beam switching with deflection angles of 15°, 30°, 45°, 60°, and 75° respectively. The calculation of transmission efficiency is the total transmission power divided by the incident power. For a metasurface design for a large deflection angle, for example, for $\theta = 60°$ the calculated FOM for the designed metasurface is about 60.76%. Due to the discrete phase distribution caused by the finite unit cell in each grating period, their FOM is not as high as the metasurface with a small deflection angle.

In this work, a tunable phase-change metasurface with a beam switching angle of 15° was fabricated as a proof of concept to demonstrate effective beam switching and splitting functions. The GST films (650 nm thickness) were deposited on a quartz substrate using an RF magnetron

sputtering system with a deposition rate of 15 nm per minute. The 160 nm thickness negative photoresist HSQ (XR-1541-006) is spin-coated on GST with 1500 rpm for 60 sec. Then, ebeam lithography is used on the samples to create the desired pattern in the area of 800 μm × 800 μm with imaging stitching. The expose dose of 7600 μC/cm^2 with an acceleration voltage of 100 kV, and a current of 500 pA is used. The sample is developed in salty developer (KOH 1%, NaCl 4%, DI 95%) for 60 seconds, and rinsed with DI water for 60 seconds. PlasmaPro System 100 Cobra ICP Etching System (700w ICP/200w RF/50sccm HBr/ 30sccm Ar/ 10mT/ 10 C) is used to etch the sample for 2 minutes to obtain the GST patterns.

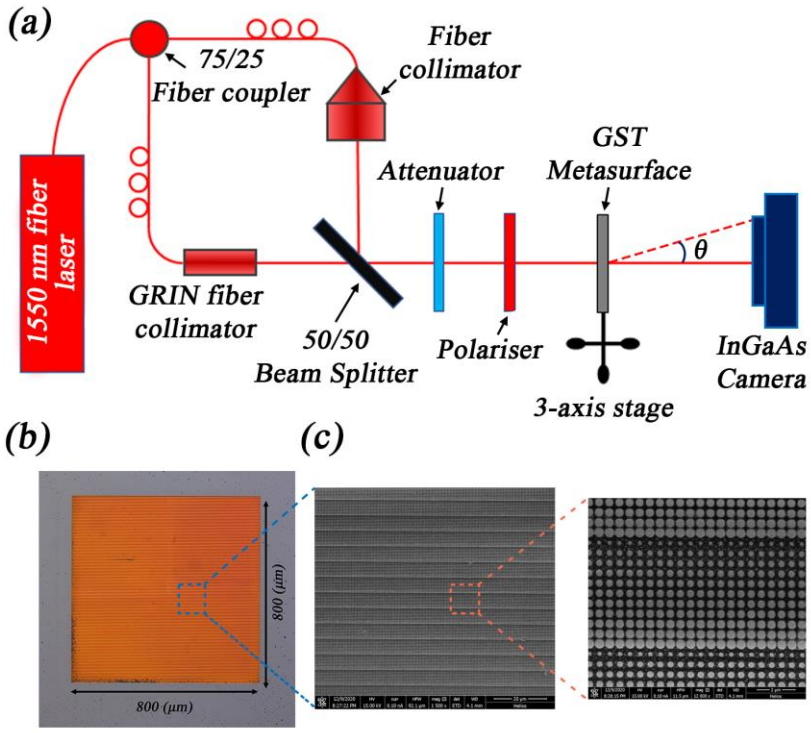

Figure 3. (a) Block diagram of the optical setup used for characterization of the phase-change metasurface. The deflection angle ($\theta = 15°$) is measured by recording the distance between the 0 and 1st order laser beams on the camera and the distance between the camera and metasurface. (b) The optical image of an 800 μm × 800 μm phase-change metasurface is fabricated by electron beam lithography. (c) The scanning electron beam (SEM) images of phase-change metasurface and the zoom-in view of a super unit cell.

The experimental setup is shown in Figure 3(a). The laser source is a femtosecond fiber laser (Calmar Laser, FPL-04CFFPM) with a central wavelength of 1550 nm and pulse width of 80 fs. It is divided into two beams by a 75/25 fiber optical coupler (Thorlabs TN1550R3F1): one is coupled into a fiber collimator (Thorlabs F280FC-1550) giving an output beam diameter of 3.6 mm for large-area illumination; the other is coupled into a single-mode pigtailed GRIN fiber collimator

(Thorlabs 50-1550A-FC) giving an output beam diameter of 600 μm for matching the GST samples (800 × 800 μm). Subsequently, these two beams can be combined by a 50/50 beam splitter (Thorlabs BSW29R), and then pass through an attenuator (in order not to saturate the image) and a linear polarizer (Thorlabs LPNIR100-MP2) to control the incident polarization state. The GST sample is placed on a rotatory stage mounted on a 3-axis mechanical stage to control its movement. The output beam diffracted from the GST sample is direct to an InGaAs camera (Photonic Science, SWIR VGA standard) without any additional optical elements in-between so that we can calculate the diffraction angle easily from the lateral shift of the laser spot captured on the camera.

Figure 3(b) shows the optical image of an 800 μm × 800 μm phase-change metasurface designed for 15° beam switching. The scanning electron microscopy image shows the top view of each unit cell in Figure 3(c).

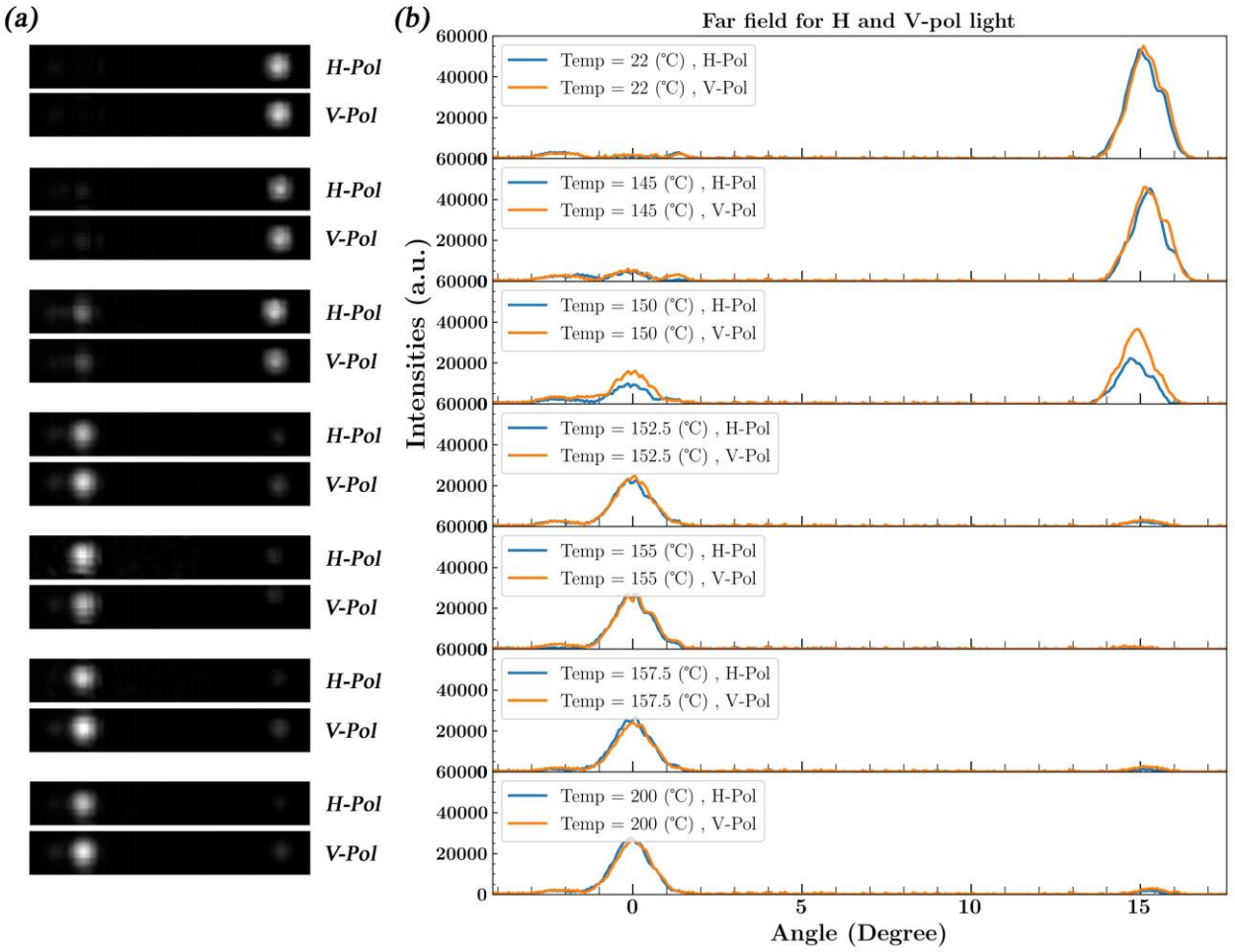

Figure 4. (a) Optical images of the split laser beam diffracted from the phase-change metasurface taken from an InGaAs camera. The sample is successively placed on the hotplate at a selected temperature

(145 °C, 150 °C, 152.5 °C, 155 °C, 157.5 °C, 200 °C) for two minutes before the characterization. (b) The intensity distribution of the transmitted beam forms the phase-change metasurface with horizontal (H) and vertical (V) polarization at various temperatures corresponding to (a). The controllable beam split ratio is achieved for different heating temperatures.

In this work, by accurate control of the GST state, the phase-change metasurface can be used as a tunable power divider controlling the ratio of the power between 0º and 15º. As shown in Figure 1(c), the optical constant of GST gradually changes as the heating temperature increases from 140 °C to 160 °C because of the partial crystallization of GST occurring in this temperature range. Above 160 °C, there is not much change in the *n-k* data due to the full crystallization of GST. We use precision temperature-controlled hotplate to gradually realize phase transition of GST metasurface from amorphous to crystalline to demonstrate controllable non-polarized beam switching and splitting. For heating temperature from 140 °C to 200 °C, the sample is placed on the hotplate at each temperature for two minutes. After that, the samples are put into the experimental setup for characterizations.

The optical images of the split laser beams diffracted from the metasurface and their intensity profiles are shown in Figures 4(a) and (b), respectively. At room temperature (22 °C) the as-prepared GST metasurface is in the amorphous state, which results in high-efficiency deflection toward 15° (1^{st} order) for both horizontal (H) and vertical (V) polarization of the laser beam. As the temperature increases from 145 °C, to 155 °C, the nucleation and growth of the crystal process begin to happen at the near-equilibrium condition with a low heating rate [48, 49]. The small increase in loss breaks the waveguide mode of the GST pillar. This hybrid phase states, from amorphous to crystalline, result in a gradual increase of intensity toward 0° (0^{th} order) and a simultaneous decrease of intensity toward 15° (1^{st} order) for both H and V polarization beams. According to experimental results, the controllable beam split ratio of 4:96 (22 °C); 11:89 (145 °C), 33:67(150 °C), 93:7 (152.5 °C), 99:1(155 °C), 97:3 (157.5 °C), and 96:4 (200 °C) are achieved for different heating temperatures. Above 155 °C, there is not much change in the beam split ratio due to the high loss of crystalline GST. Considering the beam switching toward 15° with a-GST metasurface, the directivity of 82.4% was achieved, which agrees well with the simulation results. Directivity is defined as the ratio of the transmitted beam's intensity at the desired deflection angle (15°) to the intensity of the incident beam. In practice, a more continuous and accurate beam splitting ratio could be achieved by using smaller temperature steps specifically near phase transition temperature (160 °C).

Conclusion

Taking the advantage of the very low loss GST in the amorphous state, a polarization-insensitive tunable beam switching metasurface is demonstrated with high efficiency. By changing the diameter of the a-GST nanorod, the overall phase shift of 2π is achieved for the design of a large-angle beam tuning metasurface. By transforming the GST nanorods into a crystalline state, the phase shift in the c-GST unit cell is negligible because the lossy c-GST no longer supports the waveguide mode. This results in the cancellation of the beam-steering function of the metasurface. We experimentally demonstrated the controllable beam splitting between 0° and 15° through the control of phase transition states. It is also demonstrated through simulations that a large beam steering with an angle up to 75 degrees is feasible with high efficiency. In addition, although the phase transition of metasurface was demonstrated by using thermal control, reconfigurable electrical/optical tunning is also possible for the proposed approach and platform for reversible phase change of GST metasurface [36, 53-57]. Recent studies have achieved controllable phase change metasurface through Joule heating where a 15-50 nm Al_2O_3 capping layer was deposited to protect the devices [53, 54]. A thin layer of dielectric (e.g. SiO_2 or Al_2O_3) or indium tin oxide (ITO) could be uniformly coated on the nanopillars by atomic layer deposition for optically or electrically controlled multilevel GST crystallization and reversible phase transition, respectively.

GST has been demonstrated regularly for fast switching in the range of 10-100 ns [58, 59] in memory applications, even a 500 ps phase transition of a GST cell is possible by applying a low voltage [60]. On the other hand, we note that it is still a remaining challenge to control the phase change throughout the entire metasurface device at high speed. It is expected such a challenge could be overcomed through further design optimization to achieve high modulation speed at a low voltage for possible applications in remote ranging and sensing, communication, etc.

Acknowledgments:

This work is partially supported by the Agency for Science, Technology and Research (A*STAR) under AME IRG Grant Nos. A20E5c0095, A20E5c0084 and A2083c0058, CDF Grant No. C210112044, and Ministry of Education (MOE) of Singapore AcRF Tier 3 (MOE2016-T3-1-006 (S)). Guanghui Yuan acknowledges the support from the National Innovative Talents Program of China.

References:

[1] Y. Wang *et al.*, "2D broadband beamsteering with large-scale MEMS optical phased array," *Optica*, vol. 6, no. 5, pp. 557-562, 2019.

[2] I. Kim *et al.*, "Nanophotonics for light detection and ranging technology," *Nature Nanotechnology*, vol. 16, no. 5, pp. 508-524, 2021.

[3] K. Y. Yang *et al.*, "Inverse-designed non-reciprocal pulse router for chip-based LiDAR," *Nature Photonics*, vol. 14, no. 6, pp. 369-374, 2020.

[4] D. N. Hutchison *et al.*, "High-resolution aliasing-free optical beam steering," *Optica*, vol. 3, no. 8, pp. 887-890, 2016.

[5] Y. Kurosaka *et al.*, "On-chip beam-steering photonic-crystal lasers," *Nature Photonics*, vol. 4, no. 7, pp. 447-450, 2010.

[6] A. V. Kildishev, A. Boltasseva, and V. M. Shalaev, "Planar photonics with metasurfaces," *Science*, vol. 339, no. 6125, 2013.

[7] S. B. Glybovski, S. A. Tretyakov, P. A. Belov, Y. S. Kivshar, and C. R. Simovski, "Metasurfaces: From microwaves to visible," *Physics Reports*, vol. 634, pp. 1-72, 2016.

[8] A. Arbabi, Y. Horie, M. Bagheri, and A. Faraon, "Dielectric metasurfaces for complete control of phase and polarization with subwavelength spatial resolution and high transmission," *Nature Nanotechnology*, vol. 10, no. 11, pp. 937-943, 2015.

[9] N. Yu *et al.*, "Light propagation with phase discontinuities: generalized laws of reflection and refraction," *Science*, vol. 334, no. 6054, pp. 333-337, 2011.

[10] D. Lin, P. Fan, E. Hasman, and M. L. Brongersma, "Dielectric gradient metasurface optical elements," *Science*, vol. 345, no. 6194, pp. 298-302, 2014.

[11] R. C. Devlin, A. Ambrosio, N. A. Rubin, J. B. Mueller, and F. Capasso, "Arbitrary spin-to–orbital angular momentum conversion of light," *Science*, vol. 358, no. 6365, pp. 896-901, 2017.

[12] N. I. Zheludev and Y. S. Kivshar, "From metamaterials to metadevices," *Nature Materials*, vol. 11, no. 11, pp. 917-924, 2012.

[13] M. C. Sherrott *et al.*, "Experimental demonstration of> 230 phase modulation in gate-tunable graphene–gold reconfigurable mid-infrared metasurfaces," *Nano Letters*, vol. 17, no. 5, pp. 3027-3034, 2017.

[14] A. Nemati, Q. Wang, M. Hong, and J. Teng, "Tunable and reconfigurable metasurfaces and metadevices," *Opto-Electronic Advances*, vol. 1, no. 5, p. 180009, 2018.

[15] M. Khorasaninejad and K. B. Crozier, "Silicon nanofin grating as a miniature chirality-distinguishing beam-splitter," *Nature Communications*, vol. 5, no. 1, pp. 1-6, 2014.

[16] X. Song *et al.*, "Selective diffraction with complex amplitude modulation by dielectric metasurfaces," *Advanced Optical Materials*, vol. 6, no. 4, p. 1701181, 2018.

[17] G. Kafaie Shirmanesh, R. Sokhoyan, R. A. Pala, and H. A. Atwater, "Dual-gated active metasurface at 1550 nm with wide (> 300) phase tunability," *Nano Letters*, vol. 18, no. 5, pp. 2957-2963, 2018.

[18] J. Park, J.-H. Kang, S. J. Kim, X. Liu, and M. L. Brongersma, "Dynamic reflection phase and polarization control in metasurfaces," *Nano Letters*, vol. 17, no. 1, pp. 407-413, 2017.

[19] P. Gutruf, C. Zou, W. Withayachumnankul, M. Bhaskaran, S. Sriram, and C. Fumeaux, "Mechanically tunable dielectric resonator metasurfaces at visible frequencies," *Acs Nano*, vol. 10, no. 1, pp. 133-141, 2016.

[20] S. C. Malek, H.-S. Ee, and R. Agarwal, "Strain multiplexed metasurface holograms on a stretchable substrate," *Nano Letters*, vol. 17, no. 6, pp. 3641-3645, 2017.

[21] L. Li *et al.*, "Monolithically integrated stretchable photonics," *Light: Science & Applications*, vol. 7, no. 2, pp. 17138-17138, 2018.

[22] N. A. Butakov *et al.*, "Switchable plasmonic–dielectric resonators with metal–insulator transitions," *Acs Photonics*, vol. 5, no. 2, pp. 371-377, 2018.

[23] G. Kaplan, K. Aydin, and J. Scheuer, "Dynamically controlled plasmonic nano-antenna phased array utilizing vanadium dioxide," *Optical Materials Express*, vol. 5, no. 11, pp. 2513-2524, 2015.

[24] M. Wuttig, H. Bhaskaran, and T. Taubner, "Phase-change materials for non-volatile photonic applications," *Nature Photonics*, vol. 11, no. 8, pp. 465-476, 2017.

[25] A. Nemati, W. Qian, M. Hong, and J. Teng, "Electrically tunable polarization-insensitive MIM plasmonic metasurface operating in transmission mode," *Journal of Optics*, vol. 21, no. 5, p. 055102, 2019.

[26] J. Park, J.-H. Kang, X. Liu, and M. L. Brongersma, "Electrically tunable epsilon-near-zero (ENZ) metafilm absorbers," *Scientific Reports*, vol. 5, no. 1, pp. 1-9, 2015.

[27] Y.-W. Huang *et al.*, "Gate-tunable conducting oxide metasurfaces," *Nano Letters,* vol. 16, no. 9, pp. 5319-5325, 2016.
[28] A. Nemati, Q. Wang, N. S. S. Ang, W. Wang, M. Hong, and J. Teng, "Ultra-high extinction-ratio light modulation by electrically tunable metasurface using dual epsilon-near-zero resonances," *Opto-Electronic Advances,* vol. 4, no. 7, pp. 200088-1-200088-11, 2021.
[29] N. Dabidian *et al.*, "Electrical switching of infrared light using graphene integration with plasmonic Fano resonant metasurfaces," *Acs Photonics,* vol. 2, no. 2, pp. 216-227, 2015.
[30] J. van de Groep, J.-H. Song, U. Celano, Q. Li, P. G. Kik, and M. L. Brongersma, "Exciton resonance tuning of an atomically thin lens," *Nature Photonics,* vol. 14, no. 7, pp. 426-430, 2020.
[31] S.-Q. Li, X. Xu, R. M. Veetil, V. Valuckas, R. Paniagua-Domínguez, and A. I. Kuznetsov, "Phase-only transmissive spatial light modulator based on tunable dielectric metasurface," *Science,* vol. 364, no. 6445, pp. 1087-1090, 2019.
[32] P. C. Wu *et al.*, "Dynamic beam steering with all-dielectric electro-optic III–V multiple-quantum-well metasurfaces," *Nature Communications,* vol. 10, no. 1, pp. 1-9, 2019.
[33] A. M. Shaltout *et al.*, "Spatiotemporal light control with frequency-gradient metasurfaces," *Science,* vol. 365, no. 6451, pp. 374-377, 2019.
[34] A. M. Shaltout, V. M. Shalaev, and M. L. Brongersma, "Spatiotemporal light control with active metasurfaces," *Science,* vol. 364, no. 6441, 2019.
[35] B. Gholipour, D. Piccinotti, A. Karvounis, K. F. MacDonald, and N. I. Zheludev, "Reconfigurable ultraviolet and high-energy visible dielectric metamaterials," *Nano Letters,* vol. 19, no. 3, pp. 1643-1648, 2019.
[36] Q. Wang *et al.*, "Optically reconfigurable metasurfaces and photonic devices based on phase change materials," *Nature Photonics,* vol. 10, no. 1, pp. 60-65, 2016.
[37] A. Karvounis, B. Gholipour, K. F. MacDonald, and N. I. Zheludev, "All-dielectric phase-change reconfigurable metasurface," *Applied Physics Letters,* vol. 109, no. 5, p. 051103, 2016.
[38] M. Y. Shalaginov *et al.*, "Reconfigurable all-dielectric metalens with diffraction-limited performance," *Nature Communications,* vol. 12, no. 1, pp. 1-8, 2021.
[39] K. Dong *et al.*, "A Lithography ‐ Free and Field ‐ Programmable Photonic Metacanvas," *Advanced Materials,* vol. 30, no. 5, p. 1703878, 2018.
[40] C. R. de Galarreta *et al.*, "Reconfigurable multilevel control of hybrid all-dielectric phase-change metasurfaces," *Optica,* vol. 7, no. 5, pp. 476-484, 2020.
[41] Y. Zhang *et al.*, "Broadband transparent optical phase change materials for high-performance nonvolatile photonics," *Nature Communications,* vol. 10, no. 1, pp. 1-9, 2019.
[42] C. R. de Galarreta *et al.*, "Nonvolatile reconfigurable phase ‐ change metadevices for beam steering in the near infrared," *Advanced Functional Materials,* vol. 28, no. 10, p. 1704993, 2018.
[43] J. Park *et al.*, "All-solid-state spatial light modulator with independent phase and amplitude control for three-dimensional LiDAR applications," *Nature Nanotechnology,* vol. 16, no. 1, pp. 69-76, 2021.
[44] X. Yin *et al.*, "Beam switching and bifocal zoom lensing using active plasmonic metasurfaces," *Light: Science & Applications,* vol. 6, no. 7, pp. e17016-e17016, 2017.
[45] C. H. Chu *et al.*, "Active dielectric metasurface based on phase ‐ change medium," *Laser & Photonics Reviews,* vol. 10, no. 6, pp. 986-994, 2016.
[46] C. Choi *et al.*, "Metasurface with nanostructured Ge2Sb2Te5 as a platform for broadband ‐ operating wavefront switch," *Advanced Optical Materials,* vol. 7, no. 12, p. 1900171, 2019.
[47] F. He, K. F. MacDonald, and X. Fang, "Continuous beam steering by coherent light-by-light control of dielectric metasurface phase gradient," *Optics Express,* vol. 28, no. 20, pp. 30107-30116, 2020.
[48] J. Orava, T. Wágner, J. Šik, J. Přikryl, M. Frumar, and L. Beneš, "Optical properties and phase change transition in Ge 2 Sb 2 Te 5 flash evaporated thin films studied by temperature dependent spectroscopic ellipsometry," *Journal of Applied Physics,* vol. 104, no. 4, p. 043523, 2008.
[49] G. Liang, K. Zhang, F. Zhai, H. Huang, Y. Wang, and Y. Wu, "Comparison of optical and electrical transient response during nanosecond laser pulse-induced phase transition of Ge2Sb2Te5 thin films," *Chemical Physics Letters,* vol. 507, no. 1-3, pp. 203-207, 2011.
[50] W. T. Chen, A. Y. Zhu, and F. Capasso, "Flat optics with dispersion-engineered metasurfaces," *Nature Reviews Materials,* vol. 5, no. 8, pp. 604-620, 2020.
[51] N. Yu *et al.*, "Light propagation with phase discontinuities: generalized laws of reflection and refraction," *Science,* vol. 334, no. 6054, pp. 333-7, Oct 21 2011, doi: 10.1126/science.1210713.
[52] J. R. Ong, H. S. Chu, V. H. Chen, A. Y. Zhu, and P. Genevet, "Freestanding dielectric nanohole array

metasurface for mid-infrared wavelength applications," *Optics Letters*, vol. 42, no. 13, pp. 2639-2642, 2017.
[53] Y. Zhang *et al.*, "Electrically reconfigurable non-volatile metasurface using low-loss optical phase-change material," *Nature Nanotechnology*, vol. 16, no. 6, pp. 661-666, 2021.
[54] Y. Wang *et al.*, "Electrical tuning of phase-change antennas and metasurfaces," *Nature Nanotechnology*, vol. 16, no. 6, pp. 667-672, 2021.
[55] Z. Cheng, C. Ríos, N. Youngblood, C. D. Wright, W. H. Pernice, and H. Bhaskaran, "Device‐level photonic memories and logic applications using phase‐change materials," *Advanced Materials*, vol. 30, no. 32, p. 1802435, 2018.
[56] O. Hemmatyar *et al.*, "Enhanced meta-displays using advanced phase-change materials," *arXiv preprint arXiv:2107.12159*, 2021.
[57] S. Abdollahramezani *et al.*, "Electrically driven programmable phase-change meta-switch reaching 80% efficiency," *arXiv preprint arXiv:2104.10381*, 2021.
[58] W. Wang *et al.*, "Fast phase transitions induced by picosecond electrical pulses on phase change memory cells," *Applied Physics Letters*, vol. 93, no. 4, p. 043121, 2008.
[59] G. Bruns *et al.*, "Nanosecond switching in GeTe phase change memory cells," *Applied physics letters*, vol. 95, no. 4, p. 043108, 2009.
[60] D. Loke *et al.*, "Breaking the speed limits of phase-change memory," *Science*, vol. 336, no. 6088, pp. 1566-1569, 2012.